CNPq

CBPF - CENTRO BRASILEIRO DE PESQUISAS FÍSICAS

Notas de Física

CBPF-NF-012/92

INTERMETALLIC BONDING IN SMALL PARTICLES: $Zn\ Na_8$

by

D.E. ELLIS

ABSTRACT

One electron energy levels and cohesive energies are reported for Na_8 and Zn Na_8 particles, making use of the Local Density Theory. Wavefunctions are determined in a variational Linear Combination of Atomic Orbitals approach and an interpretation of bonding is given on the basis of population analysis. Comparisons are made with predictions of the Jellium model and one-center spherical approximation models. The dominant optical absorption band of Na_8 is reproduced fairly well by *ground state* orbital energy differences. Orbital relaxation effects are studied via the transition state scheme for both optical and ionizing excitations. The calculated optical absorption of $ZnNa_8$ is compared with recent ion depletion spectroscopy results.

Key-words: Intermetallic bonding; Metal particles; Optical spectra; ionization

1. INTRODUCTION

The gradual development of experimental techniques for producing mass selected molecular beams of metal particles has provided a wealth of new data which can be used to further our understanding of intermetallic bonding. Photoelectron and photodissociation spectroscopy on neutral and charged clusters gives an important measure of electronic structure /1-3/. Photoabsorption measurements on matrix-embedded clusters and by ion depletion spectroscopy provide a complementary technique for obtaining information on optical excitations /4-5/. Up to the present very little structural information has been available, and theory has played a useful role in this area /6-8/.

Our present interest is in electronic structure and related properties of small metal particles. The alkali metals have been studied extensively by both experiment, and probably all existing theoretical methods. With a single diffuse valence electron the alkali metals provide a nearly ideal (perhaps the only) favorable case for Jellium models /6,9,10/ where nuclei and core electrons are absorbed into a featureless spherical effective potential. More sophisticated one-center approximations, such as the spherically-averaged-pseudopotential (SAPS) model can even be used to predict relative cohesive energy of different geometries /11-13/. We will not dwell here on the many theoretical studies on alkali metal particles, referring the reader to several of the seminal *ab initio* works and references cited therein /7,8,14,15/.

When one encounters bimetallic systems, especially where one component

is *not* an alkali, the very simple theoretical approaches begin to lose their appeal. Also, as the number of valence electrons grows, either with particle size or with atomic number, rigorous Configuration Interaction (CI) calculations become increasingly tedious. Although Hartree-Fock methods with effective core potentials can now be carried to rather large systems, there remain correlation errors which are difficult to estimate and correct. In the region $N \gtrsim 10$ valence electrons Local Density (LD) methods become very useful, and give predictions of reasonable quality /16-19/. In this report, we discuss the cubo-octahedral clusters Na_8 and $Zn\,Na_8$. This case is simple enough to be treated by many methods, and is currently the subject of experimental interest.

2. METHODOLOGY

The simplest spin-restricted LD formalism (Xα) was used in most cases, in which the exchange-correlation potential was approximated as

$$V_{xc} = -\alpha\left(\frac{3\rho}{8\pi}\right)^{1/3} \qquad (1)$$

with the scaling constant $\alpha=0.7$. More elaborate forms of V_{xc} could have just as easily been used, without altering the main points which we wish to

demonstrate /20-22/. Thus, the von Barth-Hedin (vBH) exchange and correlation potential was employed in some cases to check sensitivity of Xα results and to improve absolute ionization potentials values.

The eight sodium atoms were placed at the vertices of a cube, and the self-consistent-field equations were solved at a number of inter-atomic distances. In the case of Zn Na_8 the zinc atom was placed at the center of the cube. The single-particle LD orbitals were expanded in a *numerical* Linear Combination of Atomic Orbitals (LCAO) basis using the Discrete Variational Method, details of which may be found in the literature /23-25/.

In order to present the one-electron structure in compact form, partial densities of states were generated,

$$D_{\nu n\ell}(\varepsilon) = \sum_i f_{\nu n\ell,i}\, L(\varepsilon_i,\varepsilon) \quad . \qquad (2)$$

Here $L(\varepsilon_i,\varepsilon)$ is a Lorentzian line centered at the orbital energy ε_i with a full width at half maximum arbitrarily chosen equal to 0.8 eV. The amplitudes $\underset{\sim}{f}$ were determined for AO shell $(n\ell)$ of atom (ν) by a modified Mulliken population analysis of the converged self-consistent eigenvectors /26/. The net Mulliken populations are formed by multiplying $\underset{\sim}{f}$ by the corresponding orbital occupation numbers and summing over states.

Cohesive energies were calculated as the difference between the LD total energy of the cluster and a collection of noninteracting LD atoms situated at the same positions as the cluster atoms. In conjunction with a

common numerical integration grid, maximum cancellation of numerical errors is attained /27/. The statistical total energy used here was put in the convenient form

$$E_{tot} = \int \rho_\varepsilon(\vec{r})d^3r - \frac{1}{2}\left(\sum_\nu Z_\nu V'_c(\vec{R}_\nu) + \int \rho_c(\vec{r})V_c(\vec{r})\right) + \int \rho_c(\vec{r})\mathcal{U}_{xc}(\vec{r})d^3r \qquad (3)$$

Here ρ_ε is a local energy density which integrates to the one-electron energy, the terms involving V_c include nuclear-nuclear repulsion and correct for electron-electron repulsion double-counting in ρ_ε, and the last term contains the exchange-correlation energy /28/. Equ. (3) permits the identification of positive and negative contributions to cohesion for selected regions of space, such as an atomic volume.

3. RESULTS

A. Na_8

The binding energy curve obtained for the O_h cubic symmetry Na_8 cluster is shown in Fig. 1. Due to Jahn-Teller distortion it has been found by the LD PP method that the minimum energy configuration is a distorted octahedron of D_{2d} symmetry /17/. Koutecky et al. report a tetracapped tetrahedral T_d structure about ~0.1 eV lower in energy, using a CI approach. The O_h symmetry was chosen here to facilitate comparisons with the Zn-centered cluster, which was only treated in cubic symmetry. The valence orbitals

follow the expected $a_1^2 t_1^6$ pattern, giving the simple two peaked density of states. A plot of the orbital energies ε_i versus interatomic distance (Fig. 2) shows how the atomic 3s, 3p levels broaden and mix in the cluster. At the ground state equilibrium distance, level spacings and degeneracies similar to those of the one-center jellium model are obtained. Under O_h symmetry we see splittings of the order of 0.5eV with respect to spherical model degeneracies. The gradual hybridization of 3s with 3p orbitals with reducing interatomic distance is shown quantitatively in Table 1. A weak diffuse 3d contribution to the valence states is also found.

Neglecting all relaxation and final state effects we may use the ground state orbital energies $\varepsilon_i = \partial E_{total}/\partial n_i$ to estimate the first and second ionization potentials (IP) as 0.92 and 2.74 e V, see Table 2.. The experimental first IP (via appearance potentials) of ~ 4.1 e V /1,2/ is consistent with a relaxation energy of ~ 3 e V as seen in Transition State /20/ calculations on other small molecular systems, and with the near minimal basis set (1s...3spd) used here. Taking into account electronic relaxation only we obtain (see Table 4) a first IP of 3.4 e V with the Xα potential and 4.3 eV with the vBH potential. Martins et al. obtained a value of ~ 4.3 e V for the geometrically relaxed adiabatic ionization energy /17/.

A similar estimate of optical transitions would place the first dipole-allowed $4t_{1u} \Rightarrow 4t_{2g}$ excitation at ~ 2.00 e V, with the second transition $\Rightarrow 2e_g$ at 2.58 eV. A calculation of all allowed transitions up to ~5eV using dipole oscillator strengths (Table 4), predicts a double

peaked absorption, with maxima at 2.0 and 2.6eV. This compares fairly well with the observed data, showing the main peak around 494nm with (2.5 e V). Thus, a ground state calculation gives semiquantitative agreement with optical data; neither much better nor poorer than semiclassical Mie-Drude model predictions /8/. When more precise data are needed, one may of course carry out the additional excited state calculations. As shown in Table 4, electronic relaxation apparently plays a small role in these transitions among diffuse states. Geometry relaxation remains as a possibly important factor, in addition to explicit treatment of electronic correlation /8/.

B. Zn Na_8

The calculated binding energy curve for Zn Na_8 in O_h symmetry, with Zn at the cluster center is given in Fig. 3. It is immediately apparent that the Zn-centered cluster is much more rigid than the pure Na cluster. For Na_8 the curvature around equilibrium is k ~ 12 e V/a_0^2; for Zn Na_8 it is ~ 29 $\frac{eV}{a_0^2}$. Since the breathing mode vibrational frequency $\omega \sim \sqrt{k}$, there should be a dramatic change in the dynamical and ensemble thermodynamic properties of Zn-doped sodium clusters.

It is also clear that the Zn Na_8 "lattice constant" d=3.0 a_0 has increased in comparison with Na_8 (d=2.9). It is perhaps surprising that adding an atom at the cluster center produces so little expansion. However, the metallic radius of Zn of 2.6 a_0 is relatively small on the scale of Na-Na distances. The calculated cohesive energy per atom of 1.84 e V in Zn

Na_8 is almost exactly the same as for the pure Na cluster. Examination of atomic Wigner-Seitz volume contributions to cohesion (Equ. 3) shows that the Zn atomic volume is an electron acceptor (0.2e). The corresponding Mulliken charge (Table 5) is somewhat larger, 0.6e, due to contributions of diffuse s, p orbitals. The positively charged Na volumes, although reduced in size compared to the undoped cluster, showed increased cohesion. An analysis was made of the Zn-Na "bond volume" defined as lozenge-shaped regions oriented along the Zn-Na internuclear axes. The contributions to cohesion from this region of ~0.4eV are notably less than for the Na atomic volumes. Our picture of cohesion in $ZnNa_8$ is that of Zn acting as an electron acceptor, consistent with the rather larger Pauling electronegativity difference of 1.6 versus 0.9, with little direct Zn-Na bonding. The increased cohesion found in the diffuse Na volumes can be attributed to reduced electron repulsion. A orbital analysis of the Zn-Na bonding is given below, using the bond-order concept.

The single particle level structure of Zn Na_8 is interesting, and because of the Zn $3d^{10}4s^2$ atomic configuration, radically different from Jellium model predictions: a_{1g}, t_{1u}, (e_g, t_{2g}), a_{1g}, (a_{1u}, t_{1u}, t_{2u}),..., and in agreement with the SAPS model results /13/. We find that the Na_8 based $a_1^2 t_1^6$ level structure is not much altered; however it is sandwiched between the deep-lying d^{10} and Zn-4s /Na 3spd mixed highest occupied a_{1g} molecular orbital. Around equilibrium Zn retains most of its atomic structure and could be considered as a weakly coupled impurity in the "host metal". Partial densities of states (Fig. 4) and population analyses (Table 5) show

that Zn 4sp levels are actually considerably mixed with Na 3spd components.

The bond order matrix provides a convenient measure of the interaction between atoms, in terms of the charge shared between two sites. From the variational expansion of the single-particle orbitals,

$$\psi_i = \sum_j \chi_j(\vec{r}) C_{ji} \tag{4}$$

the bond order between atoms or sets p and q is defined as

$$Q_{pq} = \sum_{\substack{j \in p \\ k \in q}} \sum_i n_i \, C^{\dagger}_{ij} \, S_{jk} \, C_{ji} \tag{5}$$

$S_{jk} = \langle x_j | x_k \rangle$ is the overlap matrix, and n_i are occupation numbers. Contributions to the Zn-Na bond order from s,p and d character as well as the total, are given in Table 6. It can be seen that s-and p-bonding components increase together with decreasing distance, maintaining about the same proportion. The d-component also increases, but never really becomes significant. The steadily increasing bond charge Q(total) can be contrasted with the Wigner-Seitz volume charge q(Zn), showing transfer of charge from the Zn atomic volume into the "bond region". Of course, part of the effect is geometric, as the atomic volume shrinks with decreasing interatomic distance, and Zn remains a net electron acceptor at equilibrium.

A more pictorial view of bonding which maintains contact with the orbitals can be obtained by replacing n_i in each term of Equ. (5) by the

appropriate line-shape $L(\varepsilon_1,\varepsilon)$. The bond-order density $Q_{pq}(\varepsilon)$ for Zn-Na bond order is shown in Fig. 5. In addition to a strong bonding peak associated with the $4t_{1u}$ level which forms the HOMO in Na_8, we find a strong bonding combination in the deeper lying $3a_{1g}$(Zn s/Na s,p) state and a weak antibonding contribution in the $4a_{1g}$ HOMO. The antibonding character of the HOMO explains its weaking binding energy, and is an indication that a more stable geometry than the cubo-octahedron may exist.

The calculated ionization potentials given in Table 3 show a shift of ~2eV relative to the ground state eigenvalue. Recalling the good accuracy of the vBH potential for Na_8, one obtains a best estimate of the first-ionization bands as 2.0(a_{1g}), 3.7(t_{1u}), and 7.2(a_{1g}) eV. The last two bands correspond to the Na_8 "host" with levels stabilized by bonding with Zn; the upper level is destabilized by its antibonding character.

If this picture is correct, then all allowed optical transitions are predicted to be *autoionizing*. The first optical transition $4a_{1g} \rightarrow 5t_{1u}$ is estimated to fall at 2.11 eV using ground state orbital energies, see Table 8. Electronic relaxation via Transition State calculations produced essentially the same result (2.10 eV) in good agreement with the band at 2.15 eV obtained experimentally by ion depletion spectroscopy /29/. The second, more intense $4t_{1u} \rightarrow 5t_{2g}$ is predicted to fall at 2.20 (2.24) eV in ground (transition) state approximations. This can be identified with the experimental band centered at 2.6 eV. The fact that theoretical values predict a *red shift* of this band relative to Na_8 contrary to experiment, leads us to suppose that geometrical relaxation is important, in this case.

A third relatively intense band corresponding to $4t_{1u} \rightarrow 3e_g$ transition is calculated at 3.2 eV, and can be identified with the "new" experimental band centered at 3.0 eV.

In the present model, the "new band" is actually the $4a_{1g} \rightarrow 5t_{1u}$ first allowed transition, while the second and third experimental bands correspond to previously studied Na_8 transitions blue-shifted by bonding interaction with Zn. Further studies of $ZnNa_9$ in which different cluster symmetries and geometrical relaxation in the excited state are considered, would be useful in confirming this picture.

4. CONCLUSIONS

We have made a comparison of bonding and electronic structures of Na_8 and Zn Na_8 clusters using LD theory and an LCAO expansion basis. The value of ground state electronically relaxed Transition State levels obtained with modest basis sets in identifying and making semiquantitative predictions of IP's and optical bands has been demonstrated. In the case of a transition metal doped alkali cluster, one finds dramatic effects which arise naturally from the free atom configuration. In the case of an open shell transition metal (TM) dopant such as iron, interesting magnetic response is also expected. In studies on Fe:Be and Fe:Aℓ we find that the presence or absence of a local moment depends critically on the equilibrium impurity-host interatomic distances /30,31/. Since it is now relatively straightforward

to produce TM-alkali and TM-Aℓ mass-selected beams it should soon be possible to make more complete comparisons between theory and experiment. This could be useful in resolving some of the remaining difficulties in interpreting TM impurity data in bulk metals.

ACKNOWLEDGEMENTS

Thanks are due to Manfred Kappes for suggestions and access to unpublished data. Computations were carried out in part at the Pittsburgh Supercomputing Center under NSF support, and at Laboratório Nacional de Computação Científica, Rio de Janeiro, supported by CNPq, Brazil. This work was supported in part by the National Science Foundation, through the Northwestern University Materials Research Center, grant no. DMR 882157/, and RHAE-NM/SCT-CBPF.

FIGURE CAPTIONS

1. Cohesive Energy versus cube-edge length for cubo-octahedral Na_8.

2. Single particle energies versus cube-edge length for cubo-octahedral Na_8.

3. Cohesive Energy versus cube-edge length for cubo-octahedral $ZnNa_8$.

   F. Partial densities of states for $ZnNa_8$ at equilibrium: (a) dashed line: Zn 3d, (b) dotted line: Zn 4s, 4p, (c) dot-dash line: Na 3s, 3p.

5. Bond-order energy density of Zn-Na pair in $ZnNa_8$ at equilibrium distance.

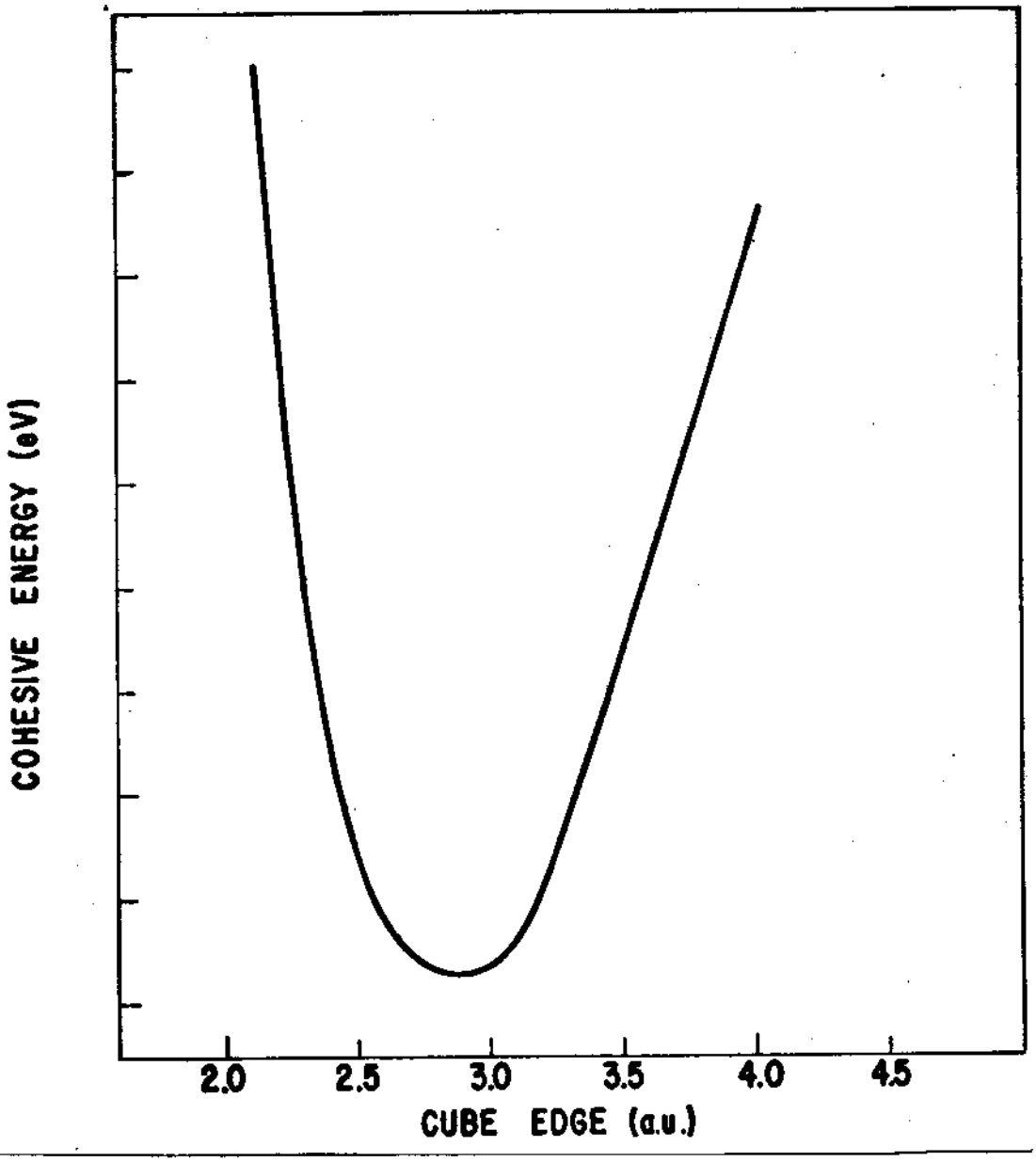

FIG. 1

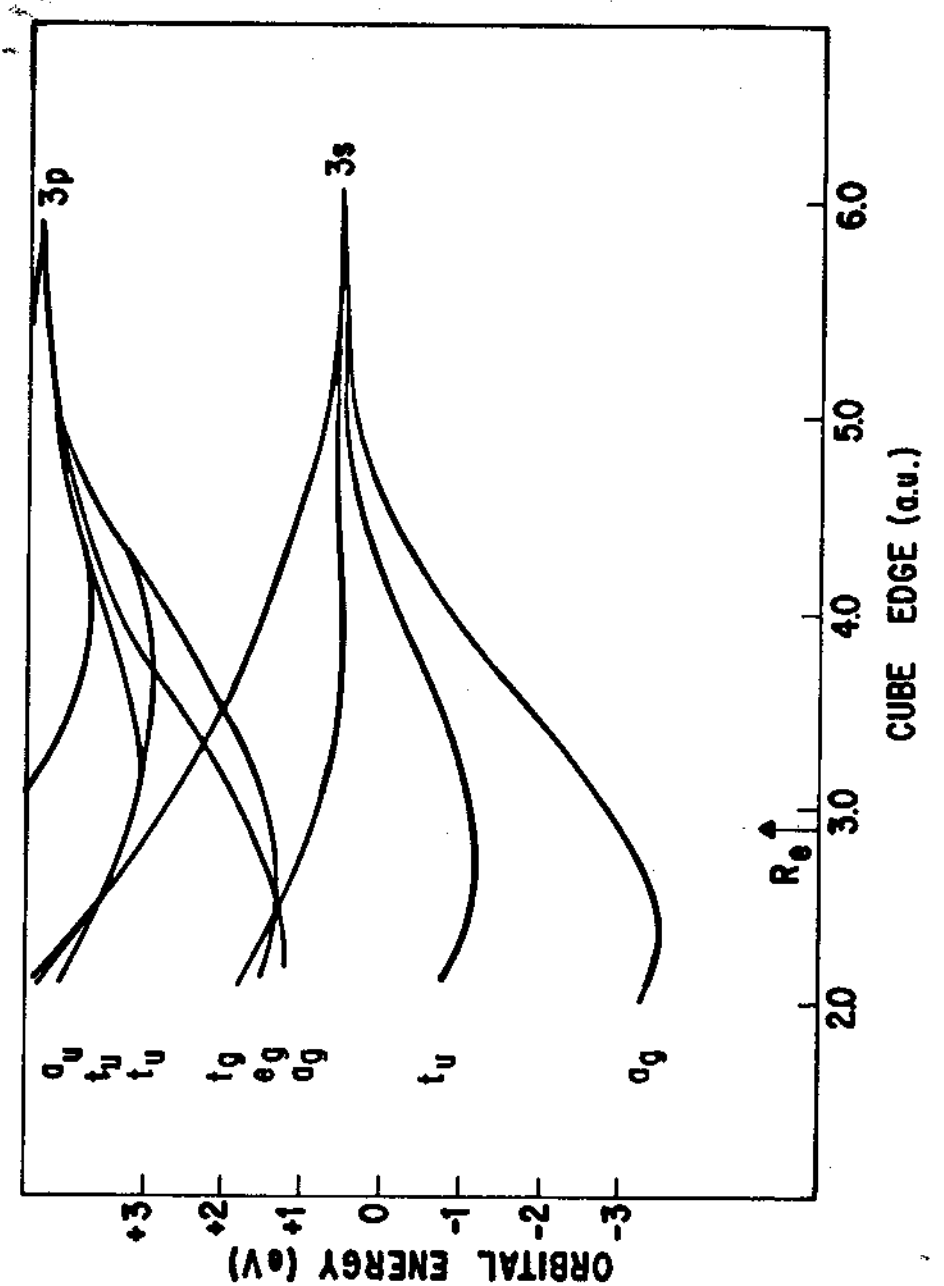
ORBITAL ENERGY (eV)
+3
+2
+1
0
-1
-2
-3
CUBE EDGE (a.u.)
2.0
3.0
4.0
5.0
6.0
R_e
3p
3s
σ_u t_{1u} t_{1u}
t_{2g} e_g σ_g
t_{1u}
σ_g

FIG. 2

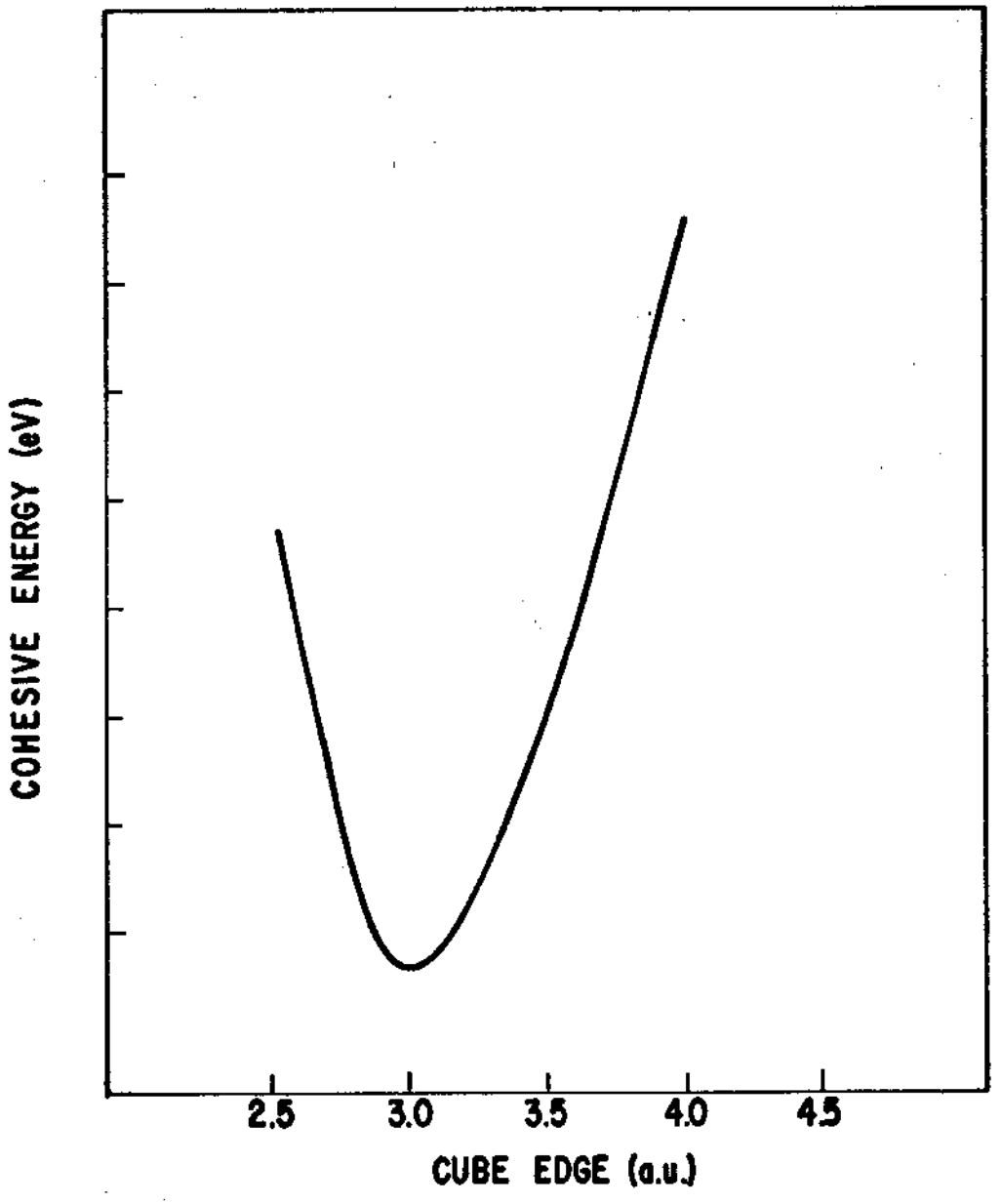

FIG. 3

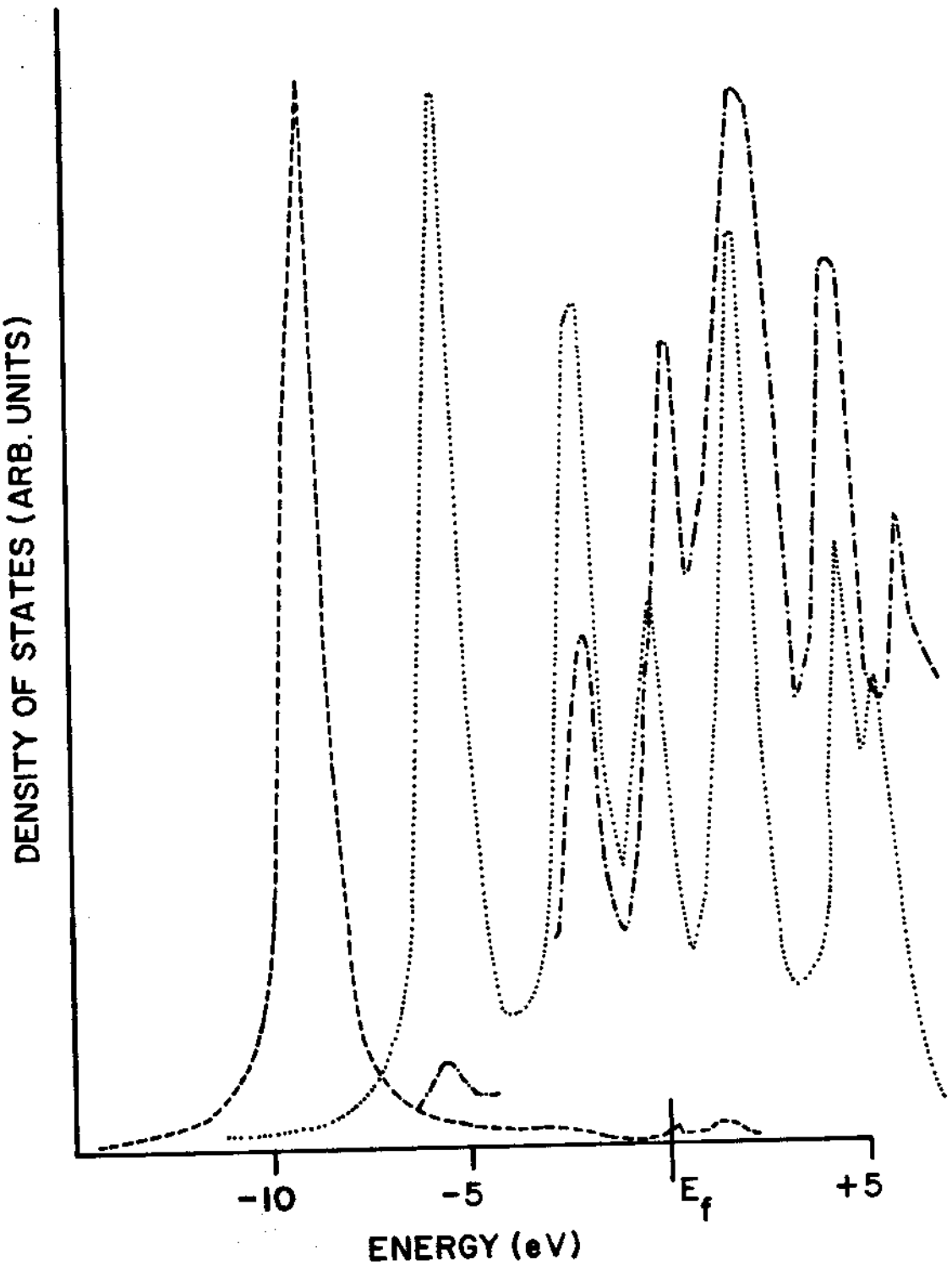

FIG. 4

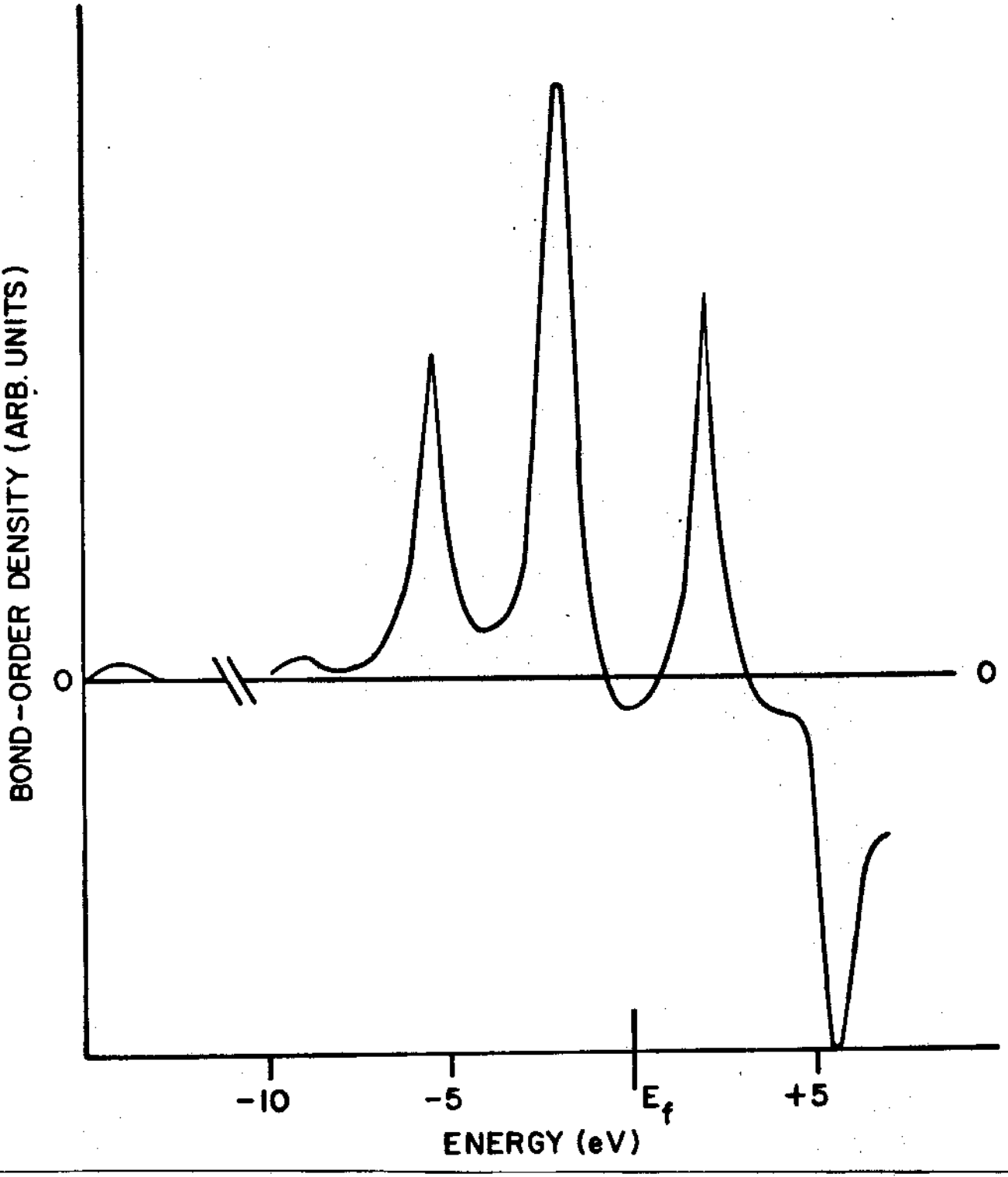

FIG. 5

Table 1: Na Mulliken atomic orbital populations versus interatomic distance (a.u.) in Na_8

R(Na-Na)	4.80	5.00	5.20	5.40	5.60	5.80[a]	6.00	6.40	6.80	7.20	7.60	8.00	9.00	10.00
3s	0.889	0.889	0.889	0.887	0.884	0.881	0.872	0.868	0.878	0.892	0.907	0.924	0.978	0.996
3p	0.115	0.112	0.110	0.111	0.113	0.115	0.122	0.124	0.114	0.100	0.085	0.068	0.018	0.003
3d	0.006	0.006	0.006	0.006	0.006	0.006	0.008	0.009	0.008	0.008	0.008	0.008	0.004	0.001

a) Calculated equilibrium distance.

CBPF-NF-012/92

Table 2: Valence and low lying excited state orbital energies (eV)and composition (per cent) for Na at equilibrium distance, using the Xα potentials

orbital	energy	s	p	d
$1a_{1g}$	-53.2[a]	100		
$2a_{1g}$	-26.0[a]		100	
$3a_{1g}$	-2.74	91	9	
$4t_{1u}$	-0.92[b]	87	12	1
$4t_{2g}$	+1.08	82	17	1
$2e_{g}$	+1.66		96	4
$4a_{1g}$	+1.95	21	67	12
$3a_{1u}$	+3.07	71	28	1
$5t_{1u}$	+3.39	19	71	10
$2t_{2u}$	+3.40		97	3
$5t_{2g}$	+5.05	10	85	5
$6t_{1u}$	+5.57	5	58	37
$3e_{g}$	+6.39		10	90

a) Representative level of narrow band.

b) Highest occupied molecular orbital.

Table 3: Calculated ionization potentials (eV) for Na_8 and $ZnNa_8$ at equilibrium distance, with Xα and vBH potentials

level	Na_8		$ZnNa_8$	
$4a_{1g}$			1.31[a]	2.00[b]
$4t_{1u}$	3.35[a]	4.28[b]	3.11	3.71
$3a_{1g}$	5.32	6.25	6.27[a]	7.23[b]
$2e_g$			9.66	14.69
$4t_{2g}$			9.68	14.73

a) Optimized level with exchange scaling α=0.7; remaining IP's estimated in nearby transition state potential

b) Optimized level with von Barth-Hedin exchange and correlation potential; remaining IP's estimated in nearby transition state potential.

Table 4: Dipole allowed optical transitions (eV) and oscillator strengths in Na_8 at equilibrium ground state distance

transition	E_{ij} [a]	$\tilde{E}_{ij}$ [b]	f_{ij}	E(expt) [c]
$4t_{1u} \Rightarrow 4t_{2g}$	2.00	2.00	5.71	2.1 [d]
$2e_g$	2.58	2.58	3.49	2.5 [e]
$4a_{1g}$	2.87			
$5t_{2g}$	5.97			
$3e_g$	7.31			
$3a_{1g} \Rightarrow 5t_{1u}$	6.13			
$6t_{1u}$	8.32			

a) Estimated from ground state eigenvalues

b) Estimated from $4t_{1g} \Rightarrow 4t_{2g}$ transition state eigenvalues.

c) Ref. 8

d) Weak, broad band. Another very weak feature is seen at ~ 1.7 e V.

e) Intense band of width ~0.2eV.

Table 5 : Zn and Na Mulliken atomic orbital populations and net charge versus interatomic distance (a.u.) in $ZnNa_8$

R(Zn-Na)		4.50	4.85	5.02	5.20[a]	5.37	5.54	5.89	6.58
Zn	3d	9.988	9.988	9.988	9.988	9.988	9.988	9.989	9.992
	4s	1.131	1.462	1.558	1.628	1.677	1.708	1.724	1.761
	4p	1.293	1.224	1.121	1.023	0.944	0.886	0.830	0.788
net		-0.411	-0.674	-0.666	-0.638	-0.609	-0.582	-0.543	-0.541
Na[b]	3s	0.735	0.741	0.756	0.773	0.788	0.800	0.820	0.842
	3p	0.212	0.165	0.148	0.134	0.122	0.113	0.100	0.080
	3d	0.028	0.024	0.022	0.020	0.019	0.017	0.013	0.011
net		0.005	0.084	0.083	0.080	0.076	0.073	0.068	0.068

a) Calculated equilibrium distance

b) 2s, 2p are also included in variational space; not shown.

Table 6: Zn-Na Bond Orders and Zn net charge versus interatomic distance (a.u.); s, p, d refers to Zn orbital character

R(Zn-Na)	Q(s)	Q(p)	Q(d)	Q(Total)	q(Zn)[b]
4.50	0.870	0.508	0.040	1.418	0.119
4.85	0.774	0.490	0.041	1.305	0.003
5.02	0.726	0.472	0.040	1.238	-0.119
5.20[a]	0.679	0.453	0.036	1.168	-0.218
5.37	0.633	0.434	0.034	1.101	-0.264
5.54	0.588	0.415	0.030	1.033	-0.308
5.89	0.509	0.378	0.024	0.911	-0.486
6.58	0.354	0.290	0.013	0.657	-0.598

a) Calculated equilibrium distance

b) Integrated charge inside "Wigner-Seitz" volume, region closest to Zn nucleus.

Table 7: Valence and low lying excited state orbital energies (eV) and composition (per cent) for $ZnNa_8$ at equilibrium distance with Xα and vBH potentials

orbital	energy α=0.7	vBH	Zn:s	p	d	Na:s	p	d
$1a_{1g}$	-52.8[a]	-53.6				100		
$2a_{1g}$	-25.9[a]	-26.2					100	
$4t_{2g}$	-7.52	-7.95			100			
$2e_g$	-7.49	-7.92			100			
$3a_{1g}$	-4.28	-4.82	63			33	4	
$4t_{1u}$	-1.09	-1.77		17		74	8	1
$4a_{1g}$	+0.59[b]	-0.15	28			38	27	7
$5t_{2g}$	+1.11	+0.26			1	81	17	1
$3e_g$	+2.12	+1.48			1		97	2
$5t_{1u}$	+2.70	+1.95		18		16	60	6
$3a_{1u}$	+2.87	+1.90				71	28	1
$2t_{2u}$	+3.32	+2.51					96	4
$6t_{1u}$	+5.08	+4.38		9		6	51	34
$5a_{1g}$	+6.03	+5.15	24				27	49

a) Representative member of narrow band of states

b) HOMO, highest occupied orbital

Table 8: Dipole allowed optical transitions E_{ij} (eV) and oscillator strengths f_{ij} in ZnNa at equilibrium ground state distance

transition	E_{ij} [a]	E_{ij} [b]	f_{ij}	E(expt) [c]
$4a_{1g} \rightarrow 5t_{1u}$	2.11	2.10	2.28	2.15[d]
$6t_{1u}$	4.53	4.54	12.27	
$7t_{1u}$	6.87	6.89		
$4t_{1u} \rightarrow 5t_{2g}$	2.20	2.24	5.76	2.62[e]
$3e_g$	3.21	3.24	3.84	2.99[f]
$6t_{2g}$	5.95	6.00	0.05	
$5a_{1g}$	7.17	7.20	0.01	
$3a_{1g} \rightarrow 5t_{1u}$	6.99	7.06		
$6t_{1u}$	9.41	9.50		

a) Estimated from ground state eigenfunctions.

b) Estimated from $4a_{1g} \rightarrow 2t_{2u}$ transition state eigenvalues.

c) Ref. 29, three Lorentzian curves were fitted to spectrum.

d) Weak band, of width ~ 0.09 eV.

e) Intense band of width 0.2 eV, blue-shifted by ~0.1 eV with respect to corresponding Na_8 band.

f) Intense band, of width ~ 0.08 eV, not present in Na_8.

REFERENCES

1. A. Herrmann, E. Schumacher, and L. Wöste, J. Chem. Phys., 68, 2327 (1978).

2. K.I. Peterson, P.D. Dao , R.W. Farley and A.W. Castleman Jr., J. Chem. Phys. 80, 1780 (1984).

3. K. Selby, M. Vollmer, J. Masui, V. Kresin, W.A. de Heer and W.D. Knight, Phys. Rev. B40, 5417 (1989).

4. M. Hoffmann, S. Lentwyler and W. Schulze, Chem. Phys. 40, 145 (1975).

5. M. Broyer, G. Delacrétaz, P. Labastie, J. Wolf and L. Wöste, Phys. Letters 57, 1851 (1986).

6. M.L. Cohen, M.Y. Chou, W.D. Knight and W.A. de Heer, J. Phys. Chem. 91, 3141 (1987); J.L. Martins, R. Car and J. Buttet, Surf. Sci. 106, 265 (1981).

7. D. Plavsic', J. Koutecky' and V. Bonacic'-Koutecky', J. Phys. Chem., 87, 1096 (1983); P. Fantucci, J. Koutecky' and G. Pacchioni, J. Chem. Phys. 80, 325 (1984).

8. V. Bonacic'-Koutecky, M.M. Kappes, P. Fantucci and J. Koutecky, Chem. Phys. Lett. 170, 26 (1990).

   J. Koutecky and P. Fantucci, Chem. Rev. 86, 539 (1986).

9. I. Katahuse, T. Ichihara, Y. Fujita, T. Matsuo, T. Sakurai and H. Matsuda, Int. J. Mass Spectro. Ion Proc. 74, 33 (1986).

10. C. Baladron and J.A. Alonso, Phys. Lett. A140, 67 (1989).

11. M.J. López, M.P. Iñiguez and J.A. Alonso, Phys. Rev. B41, 5636 (1990).

12. M.P. Iñiguez, M.J. López, J.A. Alonso and J.M. Soler, Z. Phys. D11, 163 (1989).

13. M.J. López, A. Mañanes, J.A. Alonso and M.P. Iñiguez, Z. Phys. D12, 237 (1989); J.M. López, A. Ayuela and J.A. Alonso, Ohio Supercomputer Workshop on Theory and Applications of Density Functional Approaches to Chemistry (Springer-Verlag, Berlin, to be published).

14. I. Boustani, W. Pewestorf, P. Fantucci, V. Bonacic-Koutecky and J. Koutecky, Phys. Rev. B35, 9437 (1987).

15. J. Flad, H. Stoll and H. Preuss, J. Chem. Phys. 71, 3042 (1979).

16. M. Manninen, Phys. Rev. B34, 6886 (1986).

17. J.M. Martins, J. Buttet and R. Car, Phys. Rev. B31, 1804 (1985).

18. D.R. Salahub, in "Comparison of Ab Initio Quantum Chemistry with Experiment for Small Molecules. The State et the Art", eds. W. Weltner, Jr. and R.J. Van Zee, (Reidel, Dordrecht, 1985).

19. B. Delley, D.E. Ellis, A.J. Freeman, E.J. Baerends and D. Post, Phys. Rev. B27, 2132 (1983).

20. J.C. Slater, *The Self-Consistent-Field for Molecules and Solids* (McGraw-Hill, New York, 1974).

21. J.C. Snijders and E.J. Baerends, in *Electron Distributions and the Chemical Bond*, eds. M.B. Hall and P. Coppens (Plenum, New York, 1982) p. 111.

22. W. Kohn and L.J. Sham, Phys. Rev. A140, 1133 (1965);
eds. N.M. March and S. Lundquist, *Theory of the Inhomogeneous Electron Gas*, (Plenum, New York, 1983);

U. von Barth and L. Hedin, J. Phys. C5, 1629 (1972);

O. Gunnarson and B.I. Lundquist, Phys. Rev. B13, 4274 (1976).

23. E.J. Baerends, D.E. Ellis and P. Ros, Chem. Phys. 2, 41 (1973).

24. A. Rosén and D.E. Ellis, J. Chem. Phys. 62, 3037 (1975).

25. A. Rosén, D.E. Ellis, H. Adachi and F.W. Averill, J. Chem. Phys. 65, 3629 (1976).

26. M. Press and D.E. Ellis, Phys. Rev. B35, 4438 (1987).

27. B. Delley and D.E. Ellis, J. Chem. Phys. 76, 1949 (1982).

28. D.E. Ellis, J. Guo and J.J. Low, Adv. Quantum Chem. (to be published).

29. S. Pollack, C.R.C. Wang, T. Dahlseid and M.M. Kappes (to be published).

30. D. Guenzburger and D.E. Ellis, Hyperfine Int. 60, 635 (1990).

31. D. Guenzburger and D.E. Ellis, Phys. Rev. B45, 285 (1992) and (unpublished).